Time-resolved crystallography captures light-driven DNA repair

Nina-Eleni Christou, Virginia Apostolopoulou, Diogo Melo, Matthias Ruppert, Alisia Fadini, Alessandra Henkel, Janina Sprenger, Dominik Oberthuer, Sebastian Günther, Anastasios Pateras, et al.

Title: Time-resolved crystallography captures light-driven DNA repair

Authors: Nina-Eleni Christou,[1] Virginia Apostolopoulou,[1,3] Diogo V. M. Melo,[2] Matthias Ruppert,[4] Alisia Fadini,[5] Alessandra Henkel,[1] Janina Sprenger,[1] Dominik Oberthür,[1] Sebastian Günther,[1] Anastasios Pateras,[1] Aida Rahmani Mashhour,[1] Oleksandr M. Yefanov,[1] Marina Galchenkova,[1] Patrick Y. A. Reinke,[1] Viviane Kremling,[1] T. Emilie S. Scheer,[1] Esther R. Lange,[1] Philipp Middendorf,[1] Robin Schubert,[2] Elke De Zitter,[6] Koya Lumbao-Conradson,[7,†] Jonathan Herrmann,[8] Simin Rahighi,[8,‡] Ajda Kunavar,[9,§] Emma V. Beale,[10] John H. Beale,[10] Claudio Cirelli,[10] Philip J. M. Johnson,[10] Florian Dworkowski,[10] Dmitry Ozerov,[10] Quentin Bertrand,[10] Maximilian Wranik,[10] Camila Bacellar,[10] Saša Bajt,[1,3] Soichi Wakatsuki,[8,11] Jonas A. Sellberg,[12] Nils Huse,[4] Dušan Turk,[13,14] Henry N. Chapman,[1,3,15] Thomas J. Lane[1,3,*]

Affiliations:

[1]Center for Free-Electron Laser Science CFEL, Deutsches Elektronen-Synchrotron DESY; Notkestr. 85, 22607 Hamburg, Germany

[2]European XFEL GmbH; Holzkoppel 4, 22869 Schenefeld, Germany

[3]The Hamburg Centre for Ultrafast Imaging; Luruper Chaussee 149, 22761 Hamburg, Germany

[4]Institute for Nanostructure and Solid-State Physics, CFEL Universität Hamburg; Luruper Chaussee 149, 22761 Hamburg, Germany

[5]Department of Life Sciences, Faculty of Natural Sciences, Imperial College London, London, SW7 2AZ, United Kingdom

[6]Université Grenoble Alpes, CEA, CNRS, Institut de Biologie Structurale, 38000 Grenoble, France

[7]Linac Coherent Light Source, SLAC National Accelerator Laboratory; 2575 Sand Hill Rd, Menlo Park, CA 94025, United States

[8]Department of Structural Biology, Stanford University; 318 Campus Drive West, Stanford, CA 94305-5151, United States

[9]Laboratory for Fluid Dynamics and Thermodynamics, Faculty of Mechanical Engineering, University of Ljubljana; Aškerčeva 6, 1000 Ljubljana, Slovenia

[10]Paul Scherrer Institute; CH-5232 Villigen PSI, Switzerland

[11]Stanford Synchrotron Radiation Lightsource, SLAC National Accelerator Laboratory; 2575 Sand Hill Rd, Menlo Park, CA 94025, United States

[12]Biomedical and X-ray Physics, Department of Applied Physics, AlbaNova University Center, KTH Royal Institute of Technology; S-106 91 Stockholm, Sweden

[13]Department of Biochemistry and Molecular and Structural Biology, Jožef Stefan Institute; Jamova 39, 1000 Ljubljana, Slovenia

[14]Centre of Excellence for Integrated Approaches in Chemistry and Biology of Proteins; Jamova 39, 1000 Ljubljana, Slovenia

[15]Department of Physics, Universität Hamburg; Luruper Chaussee 149, 22761 Hamburg, Germany

[†]Current Address: Department of Cardiology, University of Colorado Anschutz Medical Campus; 13001 E 17th Pl Aurora, CO 80045, United States

[‡]Current Address: Chapman University School of Pharmacy CUSP, Chapman University; Irvine, CA, 92618, USA

[§]Current Address: Department of Catalysis and Chemical Reaction Engineering, National Institute of Chemistry, Hajdrihova 19, 1001 Ljubljana, Slovenia

[*]Corresponding author. Email: thomas.lane@desy.de

Abstract: Photolyase is an enzyme that employs light to catalyze DNA repair. To capture the reaction intermediates involved in the enzyme's catalytic cycle, we conducted a time-resolved crystallography experiment. We find that photolyase traps the excited state of the active cofactor, FAD, in a highly bent geometry. This excited state performs electron transfer to damaged DNA, inducing repair. We show that the repair reaction, which involves the lysis of two covalent bonds, occurs *via* a single-bond intermediate. The resulting transformation of the substrate into product crowds the active site and disrupts hydrogen bonds with the enzyme, resulting in stepwise product release, with the 3' thymine ejected first followed by the 5' base.

One-Sentence Summary: Structures of the reaction intermediates of DNA repair by photolyase reveal the excited state of FAD, a singly bonded thymine dimer, and the mechanism of product release.

Photolyases are enzymes that repair DNA lesions induced by solar radiation, elegantly employing light to do so (*1*). The ancient origins of these enzymes suggest they were essential for early organisms to maintain genome integrity. They remain an important DNA repair mechanism in nearly all species today (*2–4*).

Distinct photolyases have evolved to repair the two most common DNA photolesions: cyclobutane pyrimidine dimers (CPD) and 6-4 adducts (*2–4*). CPDs account for ~80% of sunlight-induced DNA damage events. These lesions consist of two non-native carbon-carbon bonds between pyrimidine bases, most commonly sequence-adjacent thymines (*5–9*). CPD photolyases, which specifically target CPD lesions, break these bonds, restoring the bases to their functional structure (Fig. 1). To do so, they use a 350-450 nm photon as part of the catalytic cycle, making them one of the few known photoenzymes (*10*).

Repair of CPDs by photolyase begins with photoexcitation of a bound reduced flavin adenine dinucleotide cofactor (FADH-) (*6*, *11*), either *via* direct photon absorption by FADH- or by resonant energy transfer from a second "antenna" cofactor that harvests radiation across a wider range of the visible spectrum (*12*). Within nanoseconds, the excited state (FADH-*) transfers an electron to the CPD lesion (*7*, *13–16*). Facilitating electron transfer is a key function of the enzyme. Chemical models have shown that reduction of CPD is sufficient to break the pyrimidine dimer and produce repaired bases, even in the absence of the enzyme active site (*6*, *17–19*).

Because the FADH-* excited state decays in tens of picoseconds in solution, an important question is how the enzyme stabilizes this excited state so that electron transfer occurs before de-excitation. The ratio of electron transfer to de-excitation events is a key factor in the overall quantum efficiency, which is very high in CPD photolyases, with reported values from ~50% to >80% (*15*, *20*, *21*). In contrast, chemical models of photolyase, lacking the enzyme's structure, achieve maximum quantum efficiencies of 1-5% (*6*, *17–19*). To achieve these high quantum efficiencies, the enzyme must accommodate the transition from the ground to excited state, but then trap this state so that the de-excitation process is slower than the electron transfer timescale. The structure of this trapped intermediate, however, has to date been unknown.

Of further interest is the role of the FAD binding mode, which is distinct to the photolyase/cryptochrome family (*7–9*, *22*). The enzyme bends FAD into a U-shaped conformation (Fig. 1A), such that the FAD adenine moiety sits between the electron-donating isoalloxazine ring and the electron-accepting CPD. Spectroscopic studies have suggested that adenine mediates the electron transfer (*15*, *23*), but a precise accounting of why this U-binding mode was selected by

evolution is lacking. Structural characterization of adenine in the excited state is therefore of great interest.

After electron transfer to the CPD, the carbon-carbon bonds that form the nucleobase lesion are cleaved (*13–15*, *24*). Currently, the precise mechanism of carbon-carbon bond lysis is debated, especially whether the reaction proceeds *via* an intermediate with a single bond or, alternatively, if both bonds break simultaneously without crossing an energy barrier [see introduction of Ando *et al*., (2014), ref. (*25*)].

Finally, following CPD lysis, rapid release of the cleaved bases is essential to enable the next turnover and maximize the total number of lesions repaired. Product release occurs in ~50 µs (*1*, *9*, *26*, *27*), significantly faster than the dissociation rate for the enzyme:substrate complex, which is on the order of seconds to minutes. This increased affinity for substrate over product is clearly advantageous; however, how the enzyme's structure and dynamics enable this discrimination has not yet been accounted for.

Time-resolved crystallography targets the structural intermediates of photolyase catalysis

To determine the structure of the excited state, capture intermediates populated during CPD lysis, and characterize product release, we conducted time-resolved serial femtosecond crystallography (trSFX) experiments at the SwissFEL free-electron laser (*27*). We co-crystallized the CPD photolyase from the archaea *Methanosarcina mazei* (PL mmCPD), lacking the antenna cofactor, with a double-stranded DNA (dsDNA) substrate containing a synthetic *cis-syn* thymine dimer (a specific CPD). Prior to crystallization, protein was photoreduced and maintained in this catalytically active state using an anaerobic environment. Our crystals form an orthorhombic lattice with two protein:DNA complexes in the asymmetric unit. All results here refer to one of these two complexes, which is better ordered than its counterpart (fig. S22). Employing a viscous media injector, a stream of microcrystals embedded in a cellulose matrix was delivered to the interaction region. DNA repair was initiated by a 1.1 ps pulse of 396 nm laser light with a peak power of 360 GW cm^{-2}. This power, while sufficient to drive non-linear processes (*27–29*), produced interpretable difference map signals ($F_{o,light}$-$F_{o,dark}$). In contrast, in data obtained at 115 GW cm^{-2} the same signals could not be readily distinguished from noise (*27*).

The resulting dynamics were probed by a pulse from the XFEL at time delays ranging from 3 ps to 100 µs. To understand how photolyase interacts with the excited state FADH-*, we collected an early timepoint at 3 ps. Subsequently, to characterize CPD lysis, we collected five timepoints between 300 ps and 30 ns. Finally, to observe product release, we measured four timepoints between 1 µs and 100 µs (Fig. 1B, table S1). From the resulting diffraction data, we determined that 16-22% of the illuminated photolyase molecules undergo light-activated dynamics (*27*). By subtracting the residual non-activated signal, we computed extrapolated structure factors and used these to refine 10 time-resolved structures (*27*, *30*). We observed quantitative improvement in the models by refining against extrapolated data up to 2.1 Å to 2.4 Å depending on timepoint (table S1). However, the resulting maps and models are comparable to those determined from non-extrapolated data with a highest resolution of 2.5-3.0 Å obtained by rotational collection at a synchrotron (*27*).

Co-factor binding site facilitates dramatic butterfly bending of FADH- upon excitation

Repair chemistry begins with the photoexcitation of FADH-. To achieve high quantum efficiency, electron transfer to the substrate must be the fastest de-excitation pathway for the excited state. Transient absorption measurements show that FADH-* in solution exhibits three decay modes, with timescales of ~10 ps, ~50 ps, and ~2 ns (*31*) and relative amplitudes of 50-60%, 20-30%, and 10-15%, respectively. These same decay processes were observed in solutions of reduced flavin mononucleotide (FNMH-), which lacks adenine, demonstrating that quenching by adenine is not responsible for rapid decay (*31*). In contrast, similar to other photolyases (*15*), in the absence of substrate PL mmCPD only shows a single ~2 ns decay mode in the visible spectrum (fig. S6). The enzyme channels all excited state population into this pathway, which is sufficiently long-lived to enable productive electron transfer.

We characterized this pathway by trSFX. Before laser illumination, the FADH- cofactor is in a bent geometry, characteristic of the reduced state, with the flanking benzene and pyrimidine rings forming a +14° "butterfly bending" angle around the N5-N10 axis (Fig. 2A). 3 ps after laser excitation, this bend inverts (Fig. 2B). The sp^3-hybridized N5 and N10 centers undergo pyramidal inversion, while the benzene and pyrimidine rings, distorted from their ground-state planar geometries, kink at -23°. Spectroscopy performed by us in the absence of substrate (fig. S6) and others in both the presence and absence of substrate (*7*, *15*) suggest that FADH-* is the only populated species at 3 ps. Accordingly, we assign the flavin geometry in our 3 ps structure to the FADH-* excited state.

The photolyase FADH- binding site enables 36° of butterfly bending upon excitation, while simultaneously restricting FADH-* from reaching molecular geometries conducive to de-excitation. Butterfly bending disrupts only a single hydrogen bond between Arg378 and FAD N5 (2.9 → 4.0 Å, Fig. 2A). In contrast, all other stabilizing interactions between the protein and FAD, including hydrogen bonds with Asn403 and Asp409, are maintained upon excitation (Fig. 2A).

Ordered water molecules near the isoalloxazine readily accommodate this pronounced butterfly bending, rearranging in response to excitation and forming a new water network within 3 ps (Figs. 2A, 2C). Specifically, upon excitation, a hydrogen bond between FAD carbonyl O2 and a nearby highly coordinated water is broken as the water is displaced away from the isoalloxazine ring (2.7 Å → 3.9 Å). However, a second water strengthens its hydrogen bonding interaction with the same carbonyl (3.0 Å → 2.3 Å), simultaneously forming a new hydrogen bond with the sidechain of Ser268. These two waters are themselves hydrogen-bonded to one another both before and after their rearrangement. This water-toggle provides a second mechanism by which the FAD binding site is flexible enough to allow excitation, while simultaneously being able to form a hydrogen bond network in the excited state.

Electronic excitation disrupts adenine-associated water networks

To investigate why photolyase positions adenine between the electron-donating isoalloxazine ring and electron-accepting CPD, we interrogated our time-resolved structures for dynamics that would reveal adenine's participation in the electron transfer reaction. At 3 ps, we observe disruption of two water networks in the active site that interact strongly with this adenine (Fig. 3).

The first network consists of a five-water cluster that fills a pocket in the active site of PL mmCPD near the 3' thymine (*9*). The second network contains two adenine-associated waters that fill a small void in the protein structure on the opposite side of the adenine ring (Fig. 3). One water from each group participates in a hydrogen bond with adenine atoms N7A and N1A in the dark state.

At a 3 ps pump-probe delay, both these waters become disordered, whereas the adenine ring remains effectively stationary (Fig. 3, adenine atomic displacements ~0.2 Å). This water rearrangement propagates through the five-water cluster, disrupting a third water and inducing a 0.6 Å shift in the position of Arg256 (Fig. 3). At later timepoints, a shifting pattern of water density is observed (fig. S19), but by 10 ns, concurrent with the decay of the excited state FADH-*, both waters directly coordinating the adenine at N7A and N1A have regained order (fig. S19).

We propose three models that explain the notably specific water dynamics observed. First, electronic coupling between the adenine and isoalloxazine systems in the excited state (*32*) is sufficiently strong to disrupt adenine-water hydrogen bonding. Second, a large difference dipole on the isoalloxazine system resulting from electronic excitation perturbs these waters through space (see ref. (*33*)). Third, the adenine system is vibrationally hot, and this thermal motion disrupts these coordinated waters. Indeed, the adenine ring B-factors increase from 22 $Å^2$ to 37 $Å^2$ between the dark and 3 ps structures, *vs.* 21 $Å^2$ to 29 $Å^2$ for the isoalloxazine system, suggesting relatively increased disorder of the adenine at 3 ps (table S3). Our structure for this timepoint cannot distinguish between these models but establishes a basis upon which to design incisive future experiments and calculations that can.

Repair proceeds *via* stepwise bond-breaking of the cyclobutane pyrimidine

Between 300 ps and 3 ns we observe cleavage of the two carbon-carbon bonds that form the DNA lesion. Extrapolated polder mF_{extr}-DF_c omit maps (*27*, *34*) omitting the thymine dimer region at 300 ps and 1 ns unambiguously show that the reaction proceeds *via* a transiently populated intermediate where the C5-C5' bond is broken (Fig. 4A, fig. S17, table S2). Whether the two cyclobutane bonds break concertedly has been extensively debated (*25*), but here we provide clear structural evidence for a single-bond mechanism.

At 3 ns, the second carbon-carbon bond is broken, and the planar aromatic thymine systems are restored (Fig 4B). Between 300 ps and 3 ns, the structure of the FAD isoalloxazine ring flattens, reaching a bending angle of -4° by 3 ns (Fig. 2B), which we assign to the FADH• semiquinone state (*11*). Concomitantly, the hydrogen bond between the sidechain carbonyl of Asn403 and FAD N5 shortens (2.9 Å at 3 ps → 2.5 Å for 300 ps through 3 ns, table S3), confirming predictions from quantum calculations and IR spectroscopy measurements that predict that this interaction is essential to stabilize the semiquinone state (*35*).

Thymine dynamics after lysis drive product release

During repair, structural rearrangements of the product disrupt the geometric match between the bound bases and the relatively static active site pocket, ultimately resulting in release of the repaired thymines. Immediately after lysis, the repaired nucleobases are forced apart, rotating from a thymine/thymine angle of 43° (dark) to nearly planar (16°, 3 ns, Fig. 4B). As a result, the volume occupied by the thymine dimer increases (462 $Å^3$, dark → 475 $Å^3$, 3 ns (*27*)), crowding the active site pocket and most notably displacing Met379 (Fig. 4B).

In this geometry, the 5' thymine π-stacks against Trp305 and maintains two strong hydrogen bonding interactions with Glu301 (Fig. 4B). In contrast, rotation of the 3' thymine disrupts the most mobile piece of the active site, a hinge consisting of Arg256, Asn257, and an ordered water, which holds the 3' thymine in place prior to repair. A hydrogen bond between 3' thymine N3 and the ordered water coordinated by Asn257 is broken by 300 ps (2.9 Å, dark → 3.9 Å, 300 ps),

causing the water to become mobile and move away from the nucleobase (Fig. 4B). The Arg256-Asn257 hinge, now uncoordinated, moves towards the 5' thymine, exposing the 3' thymine to solvent and providing a clear route for product release.

Between 10 ns and 1 μs, the enzyme:product complex undergoes only minor structural variations. The initial steps of product release are observed at 10 μs, with Met379, formerly pushed out of the active site, reversing direction to move into the active site toward the 3' thymine (fig. S18). By 30 μs, this thymine flips out of the pocket completely (Fig. 5B, fig. S18, fig. S21), disrupting protein:DNA salt bridges between Arg411 and P_0 and Lys451 and P_{+1} (Fig. 5A). By 100 μs, the 5' thymine is midway through its withdrawal from the active site, and both repaired nucleobases exhibit significant disorder. In contrast, the phosphate backbone is still coordinated by salt bridges (Fig. 5C, fig. S18, fig. S21). We do not observe evidence of a restoration of Watson-Crick base pairing in our crystal structures, either because such rearrangements occur on longer timescales or are not compatible with the crystal lattice.

Our results indicate that prior to repair, the thymine dimer, with two ring systems strongly angled with respect to one another, is complementary with the active site geometry. In contrast, the repaired thymines, which adopt a planar π-stacked conformation, occupy a much larger volume in the active site and cannot form the same hydrogen bonding interactions at the 3' base, most notably with the Arg256-Asn257-water hinge system. Accordingly, thermal motion is sufficient to initiate release of the 3' base after tens of μs, followed by the 5' base hundreds of μs later (fig. S21). Due to dynamics of the bound DNA with respect to a largely static enzyme, transformation into product both swells the active site and breaks key hydrogen bonds, driving product release.

Conclusions

We have determined ten time-resolved structures of photolyase in the act of DNA repair. The observation of a highly bent excited state and single-bond thymine dimer define the key intermediates along the reaction pathway. These structures provide a foundation to understand the chemical mechanism of photolyase. Rearrangements in the DNA, in contrast with modest structural changes in the enzyme itself, drive the rate-limiting step of the catalytic cycle, which is product release. Together, our structures illuminate the function of a powerful DNA repair system, employed by nearly all lifeforms to survive and thrive under the sun.

References and Notes

1. A. Sancar, Structure and function of DNA photolyase and cryptochrome blue-light photoreceptors. *Chem Rev*. **103**, 2203–2237 (2003).
2. J. I. Lucas-Lledó, M. Lynch, Evolution of Mutation Rates: Phylogenomic Analysis of the Photolyase/Cryptochrome Family. *Mol Biol Evol*. **26**, 1143–1153 (2009).
3. Q. Mei, V. Dvornyk, Evolutionary History of the Photolyase/Cryptochrome Superfamily in Eukaryotes. *PLoS One*. **10** (2015).
4. H. S. Black, F. R. DeGruijl, P. D. Forbes, J. E. Cleaver, H. N. Ananthaswamy, E. C. DeFabo, S. E. Ullrich, R. M. Tyrrell, Photocarcinogenesis: an overview. *J Photochem Photobiol B*. **40**, 29–47 (1997).
5. A. Sancar, Mechanisms of DNA Repair by Photolyase and Excision Nuclease (Nobel Lecture). *Angewandte Chemie International Edition*. **55**, 8502–8527 (2016).
6. T. Carell, L. T. Burgdorf, L. M. Kundu, M. Cichon, The mechanism of action of DNA photolyases. *Curr Opin Chem Biol*. **5**, 491–498 (2001).
7. M. Zhang, L. Wang, D. Zhong, Photolyase: Dynamics and Mechanisms of Repair of Sun-Induced DNA Damage. *Photochem Photobiol*. **93**, 78–92 (2017).
8. A. Mees, T. Klar, P. Gnau, U. Hennecke, A. P. M. Eker, T. Carell, L. O. Essen, Crystal structure of a photolyase bound to a CPD-like DNA lesion after in situ repair. *Science*. **306**, 1789–1793 (2004).
9. S. Kiontke, Y. Geisselbrecht, R. Pokorny, T. Carell, A. Batschauer, L. O. Essen, Crystal structures of an archaeal class II DNA photolyase and its complex with UV-damaged duplex DNA. *EMBO J*. **30**, 4437–4449 (2011).
10. L. O. Björn, Photoenzymes and Related Topics: An Update. *Photochem Photobiol*. **94**, 459–465 (2018).
11. M. Maestre-Reyna, C. H. Yang, E. Nango, W. C. Huang, E. P. G. Ngurah Putu, W. J. Wu, P. H. Wang, S. Franz-Badur, M. Saft, H. J. Emmerich, H. Y. Wu, C. C. Lee, K. F. Huang, Y. K. Chang, J. H. Liao, J. H. Weng, W. Gad, C. W. Chang, A. H. Pang, M. Sugahara, S. Owada, Y. Hosokawa, Y. Joti, A. Yamashita, R. Tanaka, T. Tanaka, F. Luo, K. Tono, K. C. Hsu, S. Kiontke, I. Schapiro, R. Spadaccini, A. Royant, J. Yamamoto, S. Iwata, L. O. Essen, Y. Bessho, M. D. Tsai, Serial crystallography captures dynamic control of sequential electron and proton transfer events in a flavoenzyme. *Nat Chem*. **14**, 677–685 (2022).
12. S. Kiontke, P. Gnau, R. Haselsberger, A. Batschauer, L. O. Essen, Structural and evolutionary aspects of antenna chromophore usage by class II photolyases. *Journal of Biological Chemistry*. **289**, 19659–19669 (2014).
13. A. W. MacFarlane IV, R. J. Stanley, Cis-Syn thymidine dimer repair by DNA photolyase in real time. *Biochemistry*. **42**, 8558–8568 (2003).
14. K. Brettel, M. Byrdin, Reaction mechanisms of DNA photolyase. *Curr Opin Struct Biol*. **20** (2010), pp. 693–701.
15. M. Zhang, L. Wang, S. Shu, A. Sancar, D. Zhong, Bifurcating electron-transfer pathways in DNA photolyases determine the repair quantum yield. *Science*. **354**, 209–213 (2016).
16. C. Tan, Z. Liu, J. Li, X. Guo, L. Wang, A. Sancar, D. Zhong, The molecular origin of high DNA-repair efficiency by photolyase. *Nat Commun*. **6**, 1–6 (2015).
17. Q. H. Song, W. J. Tang, X. B. Ji, H. B. Wang, Q. X. Guo, Do photolyases need to provide considerable activation energy for the splitting of cyclobutane pyrimidine dimer radical anions? *Chemistry - A European Journal*. **13**, 7762–7770 (2007).

18. J. Butenandt, A. P. M. Eker, T. Carell, Synthesis, crystal structure, and enzymatic evaluation of a DNA-photolesion isostere. *Chemistry - A European Journal*. **4**, 642–654 (1998).
19. R. Epple, E. U. Wallenborn, T. Carell, Investigation of flavin-containing DNA-repair model compounds. *J Am Chem Soc*. **119** (1997).
20. C. Tan, Z. Liu, J. Li, X. Guo, L. Wang, A. Sancar, D. Zhong, The molecular origin of high DNA-repair efficiency by photolyase. *Nature Communications 2015 6:1*. **6**, 1–6 (2015).
21. V. Thiagarajan, S. Villette, A. Espagne, A. P. M. Eker, K. Brettel, M. Byrdin, DNA repair by photolyase: A novel substrate with low background absorption around 265 nm for transient absorption studies in the UV. *Biochemistry*. **49** (2010).
22. O. Dym, D. Eisenberg, Sequence-structure analysis of FAD-containing proteins. *Protein Science*. **10**, 1712–1728 (2001).
23. Z. Liu, X. Guo, C. Tan, J. Li, Y. T. Kao, L. Wang, A. Sancar, D. Zhong, Electron tunneling pathways and role of adenine in repair of cyclobutane pyrimidine dimer by DNA photolyase. *J Am Chem Soc*. **134**, 8104–8114 (2012).
24. V. Thiagarajan, M. Byrdin, A. P. M. Eker, P. Müller, K. Brettel, Kinetics of cyclobutane thymine dimer splitting by DNA photolyase directly monitored in the UV. **108** (2011).
25. H. Ando, B. P. Fingerhut, K. E. Dorfman, J. D. Biggs, S. Mukamel, Femtosecond stimulated Raman spectroscopy of the cyclobutane thymine dimer repair mechanism: A computational study. *J Am Chem Soc*. **136**, 14801–14810 (2014).
26. A. Espagne, M. Burdin, A. P. M. Eker, K. Brettel, Very Fast Product Release and Catalytic Turnover of DNA Photolyase. *ChemBioChem*. **10**, 1777–1780 (2009).
27. Materials and methods are available as supplementary materials.
28. M. L. Grünbein, M. Stricker, G. Nass Kovacs, M. Kloos, R. B. Doak, R. L. Shoeman, J. Reinstein, S. Lecler, S. Haacke, I. Schlichting, Illumination guidelines for ultrafast pump–probe experiments by serial femtosecond crystallography. *Nat Methods*. **17**, 681–684 (2020).
29. G. Brändén, R. Neutze, Advances and challenges in time-resolved macromolecular crystallography. *Science*. **373** (2021).
30. E. De Zitter, N. Coquelle, P. Oeser, T. R. M. Barends, J. P. Colletier, Xtrapol8 enables automatic elucidation of low-occupancy intermediate-states in crystallographic studies. *Communications Biology 2022 5:1*. **5**, 1–11 (2022).
31. Y. T. Kao, C. Saxena, T. F. He, L. Guo, L. Wang, A. Sancar, D. Zhong, Ultrafast dynamics of flavins in five redox states. *J Am Chem Soc*. **130**, 13132–13139 (2008).
32. W. Lee, G. Kodali, R. J. Stanley, S. Matsika, Coexistence of Different Electron-Transfer Mechanisms in the DNA Repair Process by Photolyase. *Chemistry - A European Journal*. **22**, 11371–11381 (2016).
33. R. F. Pauszek, G. Kodali, M. S. U. Siddiqui, R. J. Stanley, Overlapping Electronic States with Nearly Parallel Transition Dipole Moments in Reduced Anionic Flavin Can Distort Photobiological Dynamics. *J Am Chem Soc*. **138**, 14880–14889 (2016).
34. D. Liebschner, P. V. Afonine, N. W. Moriarty, B. K. Poon, O. V. Sobolev, T. C. Terwilliger, P. D. Adams, Polder maps: Improving OMIT maps by excluding bulk solvent. *Acta Crystallogr D Struct Biol*. **73**, 148–157 (2017).
35. I. M. M. Wijaya, T. Domratcheva, T. Iwata, E. D. Getzoff, H. Kandori, Single Hydrogen Bond Donation from Flavin N5 to Proximal Asparagine Ensures FAD Reduction in DNA Photolyase. *J Am Chem Soc*. **138** (2016).
36. Raw diffraction images are available via SciCAT under doi:10.16907/87a9f7a4-073e-430c-aa7f-6a194897074f.

37. Processed CrystFEL stream files are available via SciCAT under doi:10.16907/49d16998-9faf-4ae9-b48a-17aea963be65.
38. Code used for analysis and figure making is available via Zenodo under doi:10.5281/zenodo.8341840.

5

Acknowledgments: The authors would like to thank R. Stanley, D. Hekstra, M. Byrdin, K. Hadjidemetriou, G. Kurisu, W. Hinrichs, and D. Zhong for stimulating discussions and feedback, J. Maracke, L. Gumprecht, H. Fleckenstein, D. Amores, A. Zhu, F. Jabbarpour and A. Peck for technical assistance, and G. Consoli for advice concerning graphic design and presentation. Further, TL would like to acknowledge S. Boutet for mentorship and support early in the project during his time at SLAC. NC would like to thank M. Weik for his advice and encouragement. We acknowledge the Paul Scherrer Institute, Villigen, Switzerland for provision of free-electron laser beamtime at the Alvra instrument of the SwissFEL ARAMIS branch and the Helmholtz Association and DESY for core funding and infrastructure. Finally, TL and all the authors are indebted to I. Schlichting. Her constructive criticism of early versions of this manuscript singularly elevated our work.

Funding:

Helmholtz Association, Young Investigator Group (YIG) award (TL)

Swiss National Science Foundation NCCR-MUST (CB)

Göran Gustafsson Foundation, Grant No. 1808 (JA)

Carl Trygger Foundation, CTS 21:1427 (JA)

Imperial College London President's PhD Scholarship (AF)

Cluster of Excellence ‘Advanced Imaging of Matter’, Deutsche Forschungsgemeinschaft (DFG), EXC 2056, project ID 390715994. (VA, SB, HC)

National Science Foundation (USA) Graduate Research Fellowship (JH)

Department of Energy (USA), SCGSR program (JH)

Helmholtz Association, FISCOV/SFragX (PR)

Author contributions:

Conceptualization: TL

Methodology: TL, NC, DM, MR, NH

Investigation: TL, NC, DM, VA, AH, JS, DO, SG, AF, AP, AM, MG, OY, PR, VK, ES, EL, PM, JS, RS, CB, CC, EB, JHB, PJ, FD, DO, QB, MW, EDZ, DT, NH, MR, AK, JH, SR, DC, SW, SB, SB

Visualization: TL, NC

Funding acquisition: TL, HC

Project administration: TL, NC

Supervision: TL, HC

Writing: TL, NC

Competing interests: TL is an employee and shareholder of CHARM Therapeutics.

Data and materials availability: All raw diffraction data (*36*) and processed CrystFEL stream files (*37*) are available via SciCAT. Code used to perform data processing and subsequent analysis is available from Zenodo (*38*). Structure factors, maps, and determined models are available from the PDB under identifiers 8OET (dark), 8OY3 (3 ps), 8OY4 (300 ps), 8OY5 (1

ns), 8OY6 (3 ns), 8OY7 (10 ns), 8OY8 (30 ns), 8OY9 (1 μs), 8OYA (10 μs), 8OYB (30 μs), 8OYC (100 μs).

Supplementary Materials

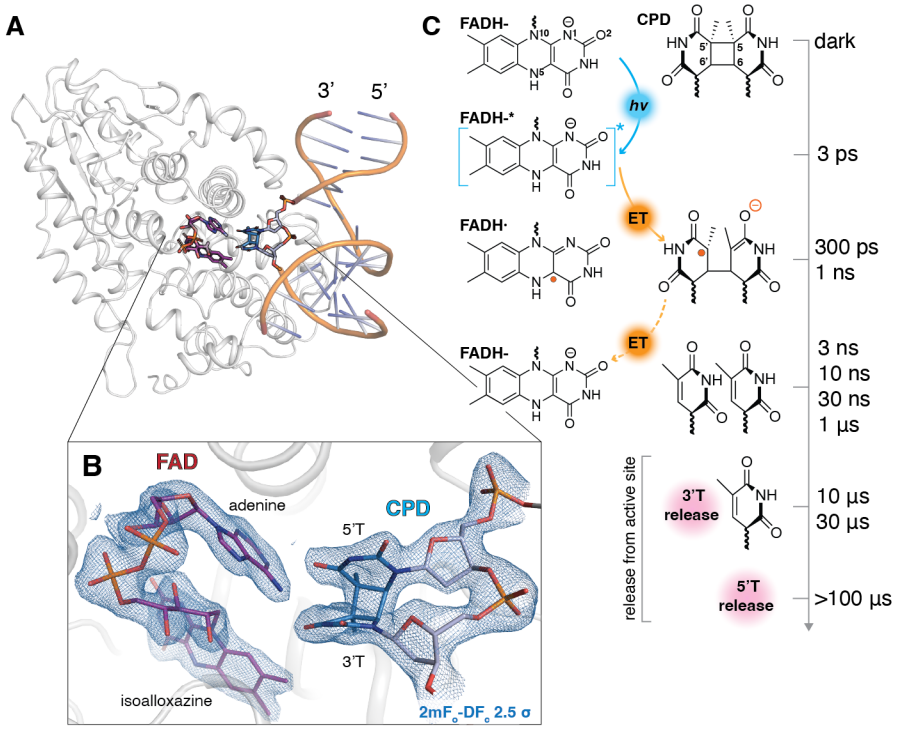

Fig. 1. The reaction cycle of DNA photolyase captured by time-resolved crystallography. (**A**) Structure of photolyase from *M. mazei*, co-crystallized with a dsDNA 14-mer containing a cyclobutane pyrimidine dimer (CPD). CPDs are DNA lesions caused by exposure to UV light. They consist of two pyrimidines, here sequence-adjacent thymines (5'T and 3'T), that are cross-linked by two non-native carbon-carbon bonds. The cross-linked thymines, incorporated into the DNA backbone by phosphodiester bonds, kink the dsDNA helix. CPD photolyases bind DNA at this kink and flip the CPD out of the double helix, positioning it adjacent to a FAD cofactor. This FAD is active when fully reduced (FADH-). Upon photon absorption, FADH- can transfer an electron to the CPD, inducing lysis in the non-native bonds and effecting DNA repair. (**B**) Region of interest showing the CPD binding mode with respect to the isoalloxazine and adenine ring systems that comprise FAD, demonstrating how adenine sits in between the FAD and CPD. Maps shown are $2mF_o$-DF_c at 2.5 σ, dark state. (**C**) Schematic of the reaction mechanism, including FAD states (left), the corresponding thymine dimer states (middle), and the pump-probe delays acquired in this study (right). Atom numbers represent indices referred to in the main text. Blue line indicates photon absorption (*hv*) and orange line electron transfer (ET), with dashes representing the possibility of electron loss resulting in a mixture of states (fig. S16, S21). At the longest timepoint studied (100 µs), the 5' thymine is only partially released, as indicated by the time axis.

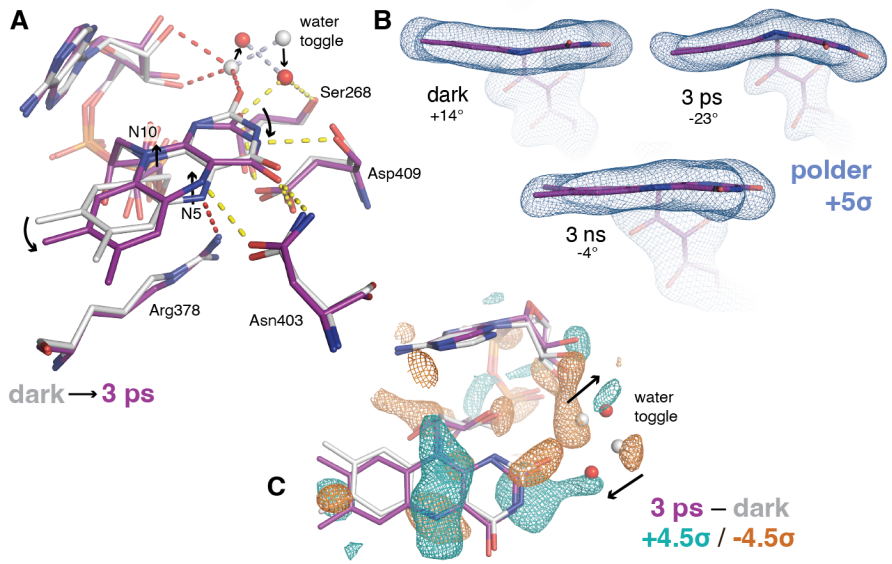

Fig. 2. FAD butterfly bending accompanies electronic excitation and subsequent electron transfer. (**A**) Excited state of FAD shown superimposed on the ground state (3 ps: purple, waters as red spheres/dark state: grey, waters as grey spheres). The FAD isoalloxazine ring participates in several hydrogen bonding interactions in both the dark and 3 ps structures. Dashed lines show hydrogen bonding interactions (yellow: present at 3 ps, red: broken between dark state and 3 ps, grey: maintained water toggle hydrogen bond). (**B**) Excitation induces severe butterfly-like bending around the N5-N10 axis of FAD, with angles indicated. Maps: extrapolated polder mF_{extr}-DF_c omit, 5 σ. Dark: fully reduced (FADH-), 3 ps: excited state (FADH-*), 3 ns: semiquinone (FADH•). (**C**) Same as (**A**), but rotated view with the isoalloxazine in the plane of the page and with $F_{o,3ps}$-$F_{o,dark}$ difference map superimposed (teal/orange, +/- 4.5 σ respectively).

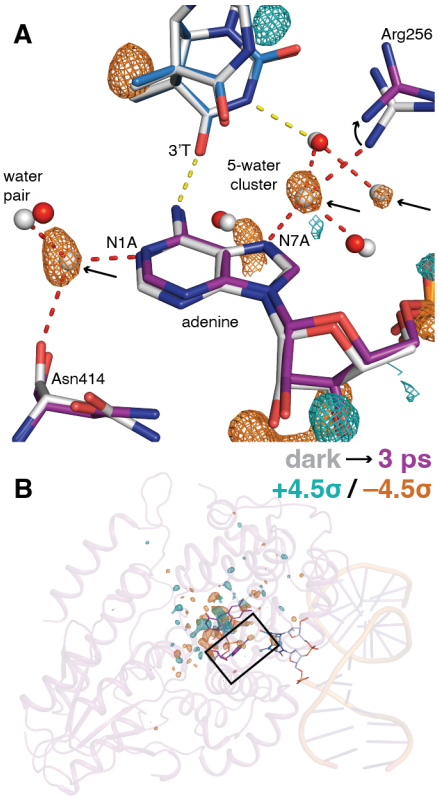

Fig. 3. Electronic excitation disrupts local water networks around adenine. (**A**) Water networks in the active site at 3 ps (3 ps: purple, red spheres/dark state: grey, grey spheres). Red dashed lines show broken hydrogen bonds, yellow dashed lines show retained hydrogen bonds. Arrows highlight key waters that become disordered following electronic excitation of FADH-, where $F_{o,3ps}$-$F_{o,dark}$ maps (teal/orange, 4.5 σ) show a loss of density. In the dark model, the N1A-water distance is 2.4 Å, and the N7A-water distance is 2.8 Å. See fig. S19 for $2mF_{extr}$-DF_c map. (**B**) The time-resolved structure at 3 ps pump-probe delay, showing $F_{o,3ps}$-$F_{o,dark}$ maps (teal/orange, 4.5 σ), indicating the adenine region of interest shown in (**A**).

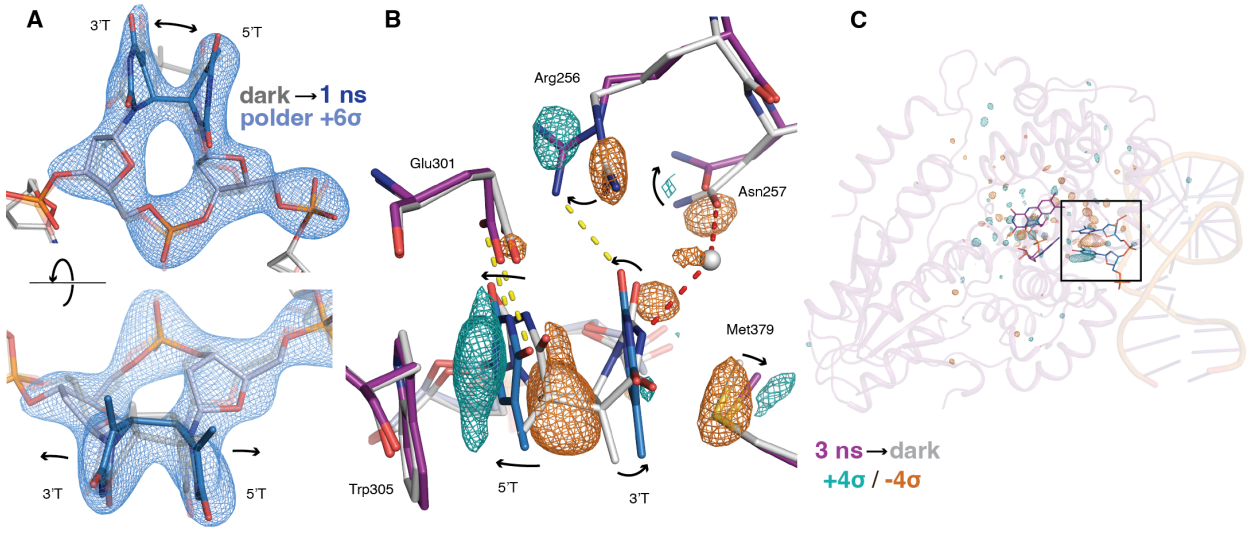

Fig. 4. DNA repair proceeds *via* a one-bond intermediate, resulting in geometric mismatch with the active site. (**A**) Extrapolated polder mF_{extr}-DF_c omit maps (blue, 6 σ) at 1 ns pump-probe delay provide evidence for a one-bond intermediate. Structure and maps for 1 ns delay in blue, dark structure with both bonds formed in grey as a reference. (**B**) By 3 ns, repair is largely complete, with thymine bases forming a coplanar, π-stacked thymine geometry (3 ns: purple, dark state: grey, water: grey sphere, teal/orange: $F_{o,3ns}$-$F_{o,dark}$ at 4 σ). This disrupts hydrogen bonding between the 3' thymine and an ordered water previously coordinated by Asn257 (red dashed lines, lost H-bonds). With this interaction disrupted, Arg256 forms a new interaction with the 5' thymine (yellow dashed lines, maintained H-bonds), weakening the interactions of the 3' thymine with the active site. (**C**) The time-resolved structure at 3 ns pump-probe delay, showing $F_{o,3ns}$-$F_{o,dark}$ maps (teal/orange, 4 σ). The CPD region of interest shown in (**A**) and (**B**) is indicated.

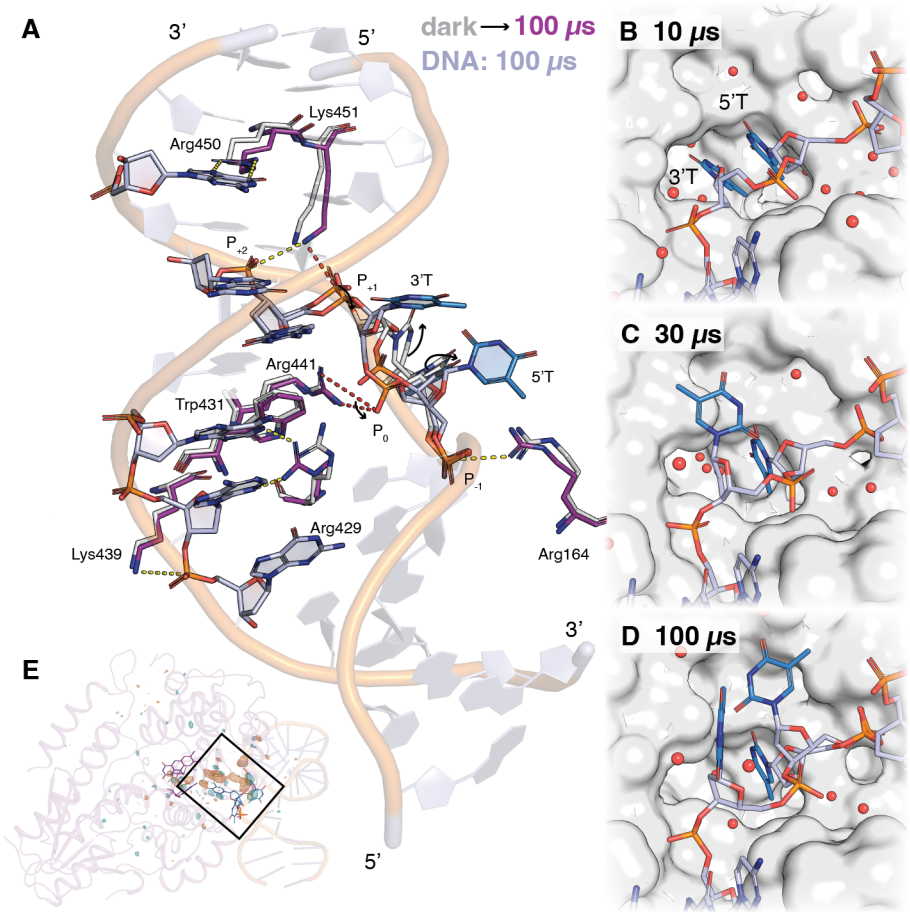

Fig. 5. Product release and disruption of DNA/photolyase interactions. (**A**) Overview of the DNA binding mode of photolyase before (dark state: grey) and after (100 μs: purple) repair. The DNA backbone conformation shown is from the structure at 100 μs. Interactions that are retained or formed at 100 μs are shown in yellow dashed lines, while interactions that are lost, most notably at the thymine dimer site (P_0-Arg441 and P_{+1}-Lys451), are shown as red dashed lines. (**B**-**D**) Product release: (**B**, 10 μs) both thymines bound in the active site, (**C**, 30 μs) 3' release, (**D**, 100 μs) partial 5' release. After exiting the active site pocket, thymines are only partially ordered: the conformations of 3' thymine at 30 μs and 5' thymine at 100 μs modeled outside of the pocket are partially occupied (figs. S18, S21). (**E**) The time-resolved structure at 100 μs pump-probe delay, showing $F_{o,100\mu s}$-$F_{o,dark}$ maps (teal/orange, 4 σ), indicating the CPD region of interest shown in (**B**-**D**).